Superlattices and Microstructures 44 (2008) 721–727

Contents lists available at ScienceDirect

Superlattices and Microstructures

journal homepage: www.elsevier.com/locate/superlattices

Simulation of the electrical characteristics of a one-dimensional quantum dot array

Wei Wang [a,b,*], Jianhui Liao [a], Jianping Sun [c], Ning Gu [a]

[a] State Key Laboratory of Bioelectronics, Jiangsu Laboratory for Biomaterials and Devices, Southeast University, Nanjing 210096, China

[b] College of Opto-electronic Engineering, Nanjing University of Posts and Telecommunications, Nanjing, 210003, China

[c] Department of Electrical Engineering and Computer Science, The University of Michigan, USA

ARTICLE INFO

Article history:
Received 1 November 2007
Received in revised form
29 August 2008
Accepted 10 September 2008
Available online 26 October 2008

Keywords:
Device simulation
Non-equilibrium Green's functions
One-dimensional quantum dot array
Quantum transport model
Linear aggregation technique

ABSTRACT

A quantum dot array, consisting of Au dots, was prepared by the linear aggregation technique and assembled between two electrodes. We study the voltage–current characteristic of the quantum dot array, using a Non-Equilibrium Green's Function (NEGF) model based on the Keldysh formalism. The results of our simulation and experimental data are compared. The simulated voltage–current curve is a reasonable fit with the measured data. It shows that the present model can be used to study quantum dot arrays. Furthermore, our results indicate that the electrical characteristics of an Au dot array are directly related to the coupling parameters.

1. Introduction

With the development of miniaturization to the nanoscale dimensions of electronic devices, transport properties of quantum-dot nanostructures have been extensively studied in recent years, due to their unique quantum characteristics. Quantum dot array systems present interesting quantization phenomena, such as Coulomb blockade, Coulomb staircase, and non-equilibrium Kondo effect [1]. Recent advances in experimental techniques made it possible to fabricate such junctions, composed of single molecules (or molecular layers) attached to two (or more) electrodes [2–9]. Exploring the use of individual molecules as active components in electronic devices has been at the

* Corresponding author at: State Key Laboratory of Bioelectronics, Jiangsu Laboratory for Biomaterials and Devices, Southeast University, Nanjing 210096, China. Tel.: +86 25 8485 5984.
E-mail address: wangwej@njupt.edu.cn (W. Wang).

0749-6036/$ – see front matter © 2008 Elsevier Ltd. All rights reserved.
doi:10.1016/j.spmi.2008.09.004

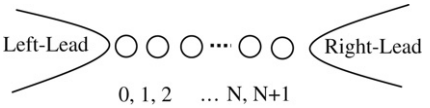

Fig. 1. The schematic drawing of one dimensional quantum dot array.

forefront of nanoelectronics research, due to the potential advantage of ultrahigh density/speed and low-cost device fabrication through self-assembly processes.

To study the transport properties of nonlinear, many-body quantum systems, such as quantum dot arrays, various approaches have been attempted, such as those based on the Wigner function, density matrix, and Non-Equilibrium Green's functions (NEGF) [10–16]. The Keldysh NEGF is known to be one of the powerful techniques to calculate quantum transport in quantum dot systems. The kinetics of the particle systems are governed by Dyson's equation, which relates the interacting Green's functions to the non-interacting Green's functions and self-energy functions. In this scheme, the electron–electron interaction is well incorporated as a term of self-energy which represents the effects on the finite device Hamiltonian, due to the outgoing wave functions from an impulse excitation within the device. The wave functions are not calculated explicitly in the device region. In addition, one advantage of this approach, is that the coupling constants between the dot and the leads do not have to be small compared with either the level spacing of the dot or thermal energy KT [17]. Therefore, the NEGF approach has gained more popularity in the past few years, which is utilized in the present work for simulation of current-voltage characteristics of one-dimensional quantum dot arrays.

Much experimental and theoretical work has been reported on nanoscale quantum dot array systems, generating very interesting results. However, little work published to date has made a comparison between experimental test data and simulation results. In the present work, we perform electron transport calculations based on the NEGF approach for a quantum dot array system, study the quantum tunneling current-voltage characteristics of the system, and make a comparison between our simulated and experimental results. The reasonable fit between the theory and experiment manifests that our simulation can provide physical insight and guidance for further experimental and theoretical studies of such quantum dot array systems, and exploration of their practical applications.

2. Method of simulation

The nonequilibrium Keldysh Green function approach has been used successfully to study the mesoscopic quantum transport of quantum dots. Consider a system of $N+2$ tunnel-coupled quantum dots, connected with two electron reservoirs, as shown in Fig. 1. The full system can be described by the Hamiltonian

$$H = \sum_{k\sigma,\alpha\in L,R} \varepsilon_{k\alpha\sigma} c^{+}_{k\alpha\sigma} c_{k\alpha\sigma} + \sum_{\sigma i=0}^{N+1} \varepsilon^{0}_{i\sigma} d^{+}_{i\sigma} d_{i\sigma} + \sum_{\sigma i=0}^{N} V_{i,i+1}(d^{+}_{i\sigma} d_{i+1,\sigma} + H.c.)$$
$$+ \sum_{k\sigma} V_L(c^{+}_{kL\sigma} d_{0\sigma} + H.c.) + \sum_{k\sigma} V_R(c^{+}_{kR\sigma} d_{N+1,\sigma} + H.c.) + \sum_{\sigma i=0}^{N+1} U_i n_{i\sigma} n_{i\bar{\sigma}} \quad (1)$$

where $c^{+}_{k\alpha\sigma}(c_{k\alpha\sigma})$ is the creation (annihilation) operator of the continuous state k in the left (right) reservoir at the energy $\varepsilon_{k\alpha\sigma}$, $d^{+}_{i\sigma}(d_{i\sigma})$ is the electron creation (annihilation) operator in the ith quantum dot region at the energy level $\varepsilon^{0}_{i\sigma}$, $V_{i,i+1,\sigma}$ is the tunneling coupling between the ith and $(i+1)$th dot, with σ being the spin index, U_i is the intradot Coulomb interaction energy of the ith dot, $n_{i\sigma} = d^{+}_{i\sigma} d_{i\sigma}$ is the electron number operator with σ on the ith dot, and $V_L(V_R)$ is the tunneling coupling between the dot $0\,(N+1)$ and the left (right) reservoir. For simplicity, we assume that there is only one localized energy level on each dot.

In order to calculate the tunneling current, we make use of the Keldysh Green's function technique [18–23], and arrive at the current through the quantum dots described by the generalized

Landauer formula [24–28]

$$J = \frac{e}{h}\sum_{\sigma}\int \mathrm{d}\varepsilon (f_L(\varepsilon) - f_R(\varepsilon))T_\sigma(\varepsilon) \tag{2}$$

where $f_L(f_R)$ is the Fermi distribution functions in the left (right) reservoir, e.g.

$$f_{L(R)}(\varepsilon) = \frac{1}{\exp(\frac{\varepsilon-\mu_{L(R)}}{kT})+1}, \tag{3}$$

$\mu_{L(R)}$ is the chemical potential in the left (right) reservoir, $T_\sigma(\varepsilon)$ is the transmission probability, as given by

$$T_\sigma(\varepsilon) = \mathrm{Tr}[\Gamma^L(\varepsilon)G^r_\sigma(\varepsilon)\Gamma^R(\varepsilon)G^a_\sigma(\varepsilon)] \tag{4}$$

where the components of the retarded and advanced Green's functions are defined as $G^{r,a}_{ij\sigma}(t) = \langle\langle d_{i\sigma}(t)|d^+_{j\sigma}(0)\rangle\rangle^{r,a} = \mp \mathrm{i}\theta(\pm t)\langle\{d_{i\sigma}(t), d^+_{j\sigma}(0)\}\rangle$, with $\theta(t)$ being the step function. The energy representation of Green's functions can be obtained using Fourier transforms for time representation. $\Gamma^{L(R)}(\varepsilon)$ denotes the coupling strength matrix, which is defined as $(\Gamma^{L(R)})_{ij} = \Gamma_{0(N+1)}\delta_{0(N+1),i}\delta_{0(N+1),j}$. $\Gamma_{0(N+1)}$ denotes the coupling strength of the dot 0 $(N+1)$ to the left (right) lead. Therefore, the transmission probability can be simply expressed as $T_\sigma(\varepsilon) = \Gamma_{N+1}\Gamma_0|G^r_{0,N+1\sigma}|^2$.

To calculate $T_\sigma(\varepsilon)$, we need to evaluate Green's functions $G^r_{ij\sigma}(\varepsilon)$. By applying the method of EOM and Keldysh's contour integration technique [10,29,30], the equations about Green function $G^r_{ij\sigma}(\varepsilon)$ can be written as

$$\begin{aligned}(\varepsilon - \varepsilon_i + \mathrm{i}\Gamma_0\delta_{i0} + \mathrm{i}\Gamma_{N+1}\delta_{i,N+1})G^r_{ij\sigma}(\varepsilon) &= \delta_{ij} + U_iG^r_{ij\sigma\bar\sigma}(\varepsilon) + V_{i-1,i}(1-\delta_{i0})G^r_{i-1,j\sigma}(\varepsilon)\\ &\quad + V^*_{i,i+1}(1-\delta_{i,N+1})G^r_{i+1,j\sigma}(\varepsilon).\end{aligned} \tag{5}$$

In the above equations, the two-particle retarded Green's function $G^r_{ij\sigma\bar\sigma}(\varepsilon)$ is involved, and $G^r_{ij\sigma\bar\sigma}(\varepsilon)$ is defined as $G^r_{ij\sigma\bar\sigma}(\varepsilon) = \langle\langle d_{i\sigma}n_{i\bar\sigma}|d^+_{j\sigma}\rangle\rangle^r$. Writing the equation of motion for the two-particle retarded Green's function and considering the Hartree–Fock approximation, one obtains the following expression

$$\begin{aligned}(\varepsilon - (\varepsilon_i + U_i) + \mathrm{i}\Gamma_0\delta_{i0} + \mathrm{i}\Gamma_{N+1}\delta_{i,N+1})G^r_{ij\sigma\bar\sigma}(\varepsilon) &= \langle n_{i\bar\sigma}\rangle\delta_{ij} + V_{i-1,i}(1-\delta_{i0})\langle n_{i\bar\sigma}\rangle G^r_{i-1,j\sigma}(\varepsilon)\\ &\quad + V^*_{i,i+1}(1-\delta_{i,N+1})\langle n_{i\bar\sigma}\rangle G^r_{i+1,j\sigma}(\varepsilon).\end{aligned} \tag{6}$$

Substituting Eq. (6) into Eq. (5), after performing some algebra operations, we obtain the iterative equation about Green function $G^r_{ij\sigma}(\varepsilon)$

$$\begin{aligned}&\left(\frac{\langle n_{i\bar\sigma}\rangle U_i}{\varepsilon - \varepsilon_i - U_i + \mathrm{i}\Gamma_0\delta_{i0} + \mathrm{i}\Gamma_{N+1}\delta_{i,N+1}} + 1\right)V_{i-1,i}(1-\delta_{i0})G^r_{i-1,j\sigma}(\varepsilon)\\ &- (\varepsilon - \varepsilon_i + \mathrm{i}\Gamma_0\delta_{i0} + \mathrm{i}\Gamma_{N+1}\delta_{i,N+1})G^r_{ij\sigma}(\varepsilon)\\ &+ \left(\frac{\langle n_{i\bar\sigma}\rangle U_i}{\varepsilon - \varepsilon_i - U_i + \mathrm{i}\Gamma_0\delta_{i0} + \mathrm{i}\Gamma_{N+1}\delta_{i,N+1}} + 1\right)V^*_{i,i+1}(1-\delta_{i,N+1})G^r_{i+1,j\sigma}(\varepsilon)\\ &= -\delta_{ij}\left(1 + \frac{\langle n_{i\bar\sigma}\rangle U_i}{\varepsilon - \varepsilon_i - U_i + \mathrm{i}\Gamma_0\delta_{i0} + \mathrm{i}\Gamma_{N+1}\delta_{i,N+1}}\right).\end{aligned} \tag{7}$$

The average electron occupation number of electron with spin σ, can be solved in a self-consistent manner using the following relation [29]

$$\langle n_{i\sigma}\rangle = -\mathrm{i}\int\frac{\mathrm{d}\varepsilon}{2\pi}G^<_{ii\sigma}(\varepsilon) \tag{8}$$

where the lesser Green's functions are defined as $G^<_{ii\sigma}(t) = \mathrm{i}\langle d^+_{i\sigma}(0)d_{i\sigma}(t)\rangle$, in which the lesser Green's function matrix in energy space is given by the Keldysh equation $G^<_\sigma(\varepsilon) = G^r_\sigma(\varepsilon)\Sigma^<(\varepsilon)G^a_\sigma(\varepsilon)$, with the lesser self-energy takes on simple form $\Sigma^<(\varepsilon) = \mathrm{i}(f_L(\varepsilon)\Gamma^L(\varepsilon) + f_R(\varepsilon)\Gamma^R(\varepsilon))$.

To calculate the electric current J, we need to obtain the retarded Green's function $G^r_\sigma(\varepsilon)$ and the average electron occupation number of electron $\langle n_{i\sigma}\rangle$ by solving Eqs. (7) and (8) self-consistently.

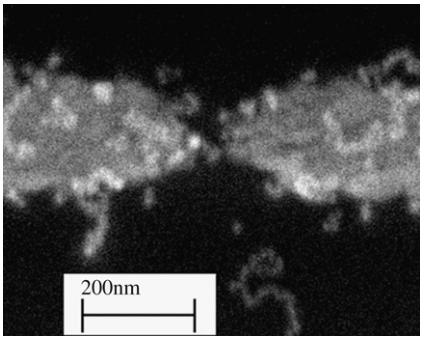

Fig. 2. The SEM photograph of gold nanoparticle chains between two electrodes.

3. Experiment

The fabrication of the Au dot array was done by two techniques [31–33]. First the linear aggregation technique was used to form Au colloidal particles in organic solution. Second, a molecular self-assembly technique was adopted to attach the Au dot array in between two electrodes. A Au–dithiol–nanocluster–dithiol–Au device resulted from these procedures.

A silicon wafer with 200 nm thick native oxide served as a substrate on which leads were presented. To create a gap of nanometer scale separation, the leads were formed using electron beam lithography and shadow evaporation. In the process, metal was shadow evaporated to give 5 nm Cr and 25 nm Au in thickness. Then Au bonding pads were defined using optical lithography on the silicon substrate; 20 nm Cr and 80 nm Au were evaporated onto the sample.

The sample was exposed to ultraviolet radiation for 30 min and immersed in an ethanol bath for 10 min in order to remove organic impurities on the surface of sample. Subsequently, the sample was immersed in a solution of 1 mmol/L 1,6-hexanedithiol for 24 h. Then, the sample was rinsed with two ethanol baths. The linear dithiol binds one of their end to the Au surface, thereby forming a monolayer. The sample was then transferred to a solution of Au nanocrystals for 24–72 h. During this step, the nanocrystals bind to the exposed end groups of the linker molecules which envelope the Au leads. The morphology of nanoparticle aggregates was characterized with a scanning electron microscope (see Fig. 2).

Current-voltage characteristics of the quantum dot device were measured in a shielded room, using a precision semiconductor parameter analyzer (Keithley 4200 Semiconductor Characterization System) at room temperature. The measured I–V curve is shown in Fig. 3 (solid line).

4. Simulation and discussion

In our numerical calculations, we assume that the quantum dot array is a one dimensional array and there is one energy level in every quantum dot, i.e. $\varepsilon_0^0 = \varepsilon_1^0 = \varepsilon_2^0 = \cdots = \varepsilon_N^0 = \varepsilon_{N+1}^0$. For simplicity, we assume that the Fermi level at the right hand side is fixed ($\mu_R = 0$). When a bias V is applied between two leads, the Fermi level of the left lead is $\mu_L = -$eV. In the wide-band limit, line width function Γ_0 and Γ_{N+1} are energy-independent constants and we assume $\Gamma_0 = \Gamma_{N+1} = \Gamma$.

Assuming the radius of the gold particles between two electrodes to be 3 nm, the effective capacitance C of each gold island is estimated to be $4\pi\varepsilon_0\varepsilon_r r \approx 0.87 \times 10^{-18}$ F, where r is the radius of the gold particles, ε_0 is the vacuum dielectric constant, and we assume that the dielectric constant of the organic tunnel barrier 2.6 [33]. Therefore, the Coulomb interaction energy of quantum dots can be estimated as $U = e^2/C \approx 0.18$ eV, which is larger than thermal energy at room temperature (26 meV). In the following calculation, we have $U_0 = U_1 = \cdots = U_N = U_{N+1} = U$.

From the experimental curve in Fig. 3, we notice that the I–V curve is asymmetric with respect to the zero bias. We can see step-like structures under negative bias. The I–V curve shows a step-like feature, with the steps more pronounced for negative voltages than for positive ones. The currents

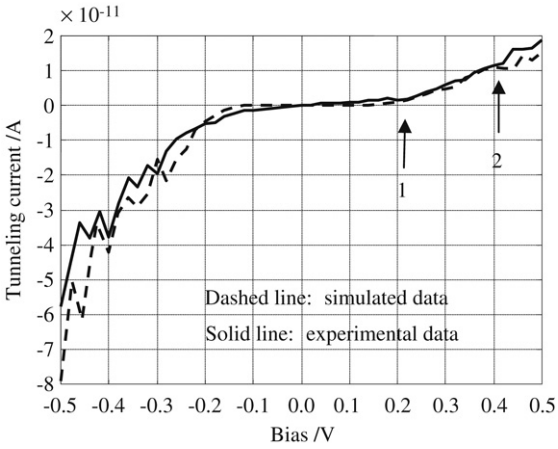

Fig. 3. The comparison of tunneling current for 7 quantum dot array with calculated data and experimental data. The parameters used in the calculations are: $\varepsilon_i^0 = 0.20$ eV for any i and $\Gamma = 65$ meV.

in the positive bias region are lower than those in the negative bias region. The positive threshold voltage is larger than the negative one. To compare with experimental current data, we apply the NEGF technique to simulate I–V characteristics, using V_{ij} and N as fitting parameters.

From Fig. 2, the gap between the two electrodes is about 80 nm. We estimate that the number of dots in 1D quantum dot array is between 5 and 15. At first, the number of dots is taken to be 15. The computed currents are found too small for experimental data. With a decreasing the number of dots, the computed currents increase. The amplitude and shape of the current curve is very sensitive to the dot number and tunneling coupling V_{ij}, respectively. We adjust these by making the best fit to the experimental curve. We found an optimized fit with $N = 5$ and $V_{01} = 23.0\Gamma$, $V_{12} = 49.0\Gamma$, $V_{23} = 1.50\Gamma$, $V_{34} = 0.045\Gamma$, $V_{45} = 0.040\Gamma$, $V_{56} = 0.020\Gamma$, $\Gamma = 65$ meV. The simulated curve is shown in Fig. 3 (dashed line).

The asymmetric features of the tunneling current characteristics described above can be explained with Keldysh Green's function model. Under positive bias, electrons enter the dot array from the right-side lead. When they arrive at the 6th dot, most of electrons bounce back, due to smaller $V_{N,N+1}$ leading to a lower tunneling current, and most electrons from the right-hand side lead only see one energy level of one dot, $\varepsilon_6^0 = 0.20$ eV. It is found that, at positive bias, the I–V curve exhibits mainly a step-like structure due to Coulomb blockade, which correspond to the electron resonant tunneling through the quantum dots at energy level ε_6^0 and the new sub-level $\varepsilon_6^0 + U$ created by Coulomb interaction effects. The arrow 1 and arrow 2 in Fig. 3 denote the two resonant positions, respectively. With increasing bias, when a resonant level crosses the Fermi level of the source electrode, the current curve shows a step-like structure.

With negative bias, most electrons enter the dot array from left lead, due to larger V_{01} (the tunneling coupling between the 0-th dot and the first dot). So the tunneling current is higher with a negative bias. Most electrons see the other $N + 1$ quantum dots. Since the $N + 1$ interdots are coupled, $N + 1$ states are mixed up and form the new energy structure different from that of a single dot. Moreover, each energy level brings about a sub-level due to Coulomb interaction effects. In this case, energy levels in the quantum system form a complex energy spectrum. Consequently, in the low current region, some levels are open to accept electrons. By increasing the bias voltage, a multiple step-like current feature appears when it flows through the resonant levels which reside between the Fermi level of left and right electrodes.

To validate this view, we calculate the electronic charge of dots. Fig. 4 shows the electronic charge for quantum dots in different biases. The following observations are made from the calculated results: (1) With negative bias, the charge values are larger than that with positive bias. The electrons go into the array from the left-side lead easily, so a large number of electrons accumulate in the dots, and

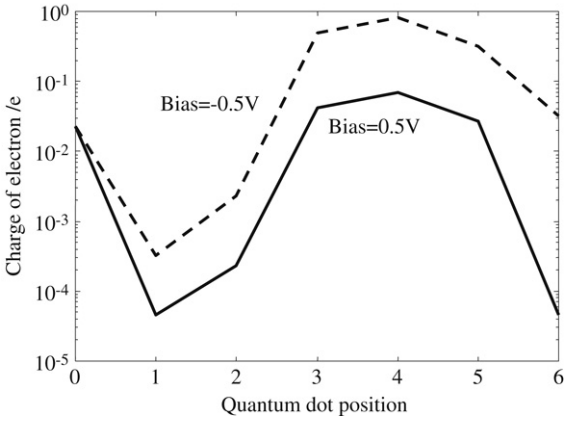

Fig. 4. The charge of electron for $N + 2$ quantum dots.

charging effects appear in the I–V curve. Hence the I–V curve shows the rich step-like structures. (2) With positive bias, since the tunneling electrons see fewer energy levels, the electrons cannot easily accumulate in the dots and the I–V curve shows a simple step-like structure due to resonant tunneling. The analysis result is consistent with the above explanations.

Our calculated result resembles the experimental data with low bias, but the experimental data is larger than the modeled data with large bias. The discrepancy can be resulted from several approximations in our calculations, including that there is only one energy level in every quantum dot, and that the current through higher energy levels was not taken into account. In fact, the electronic structures of quantum dots play an important role in the determination of the tunneling current of quantum dots. In addition, the bias-dependent tunneling coupling matrix $\Gamma^{L(R)}$ was not taken into account in the present calculation.

5. Conclusion

In this work, gold quantum dot arrays are prepared by a linear aggregation technique, and they are assembled between the two electrodes. Their voltage–current characteristics are measured. These quantum dot arrays are studied using numerical simulations based on the Keldysh NEGF approach. Our computational results are in reasonably good agreement with experimental data. Our results show that the electrical characteristics of gold quantum dot arrays are directly related to the coupling parameters between the dots. As the inter-dot coupling can be controlled in experiments [34], this approach may be used to provide an analysis tool and design aid for quantum dot device development.

Acknowledgments

This work was supported by the National Natural Science Foundation of China (Grant nos. 60371037, 20573019, 90406023, 90406024) and the Foundation of State key Laboratory of Electronic Thin Films and Integrated Devices (No. KF2007001).

References

[1] O. Entin-Wohlman, A. Aharony, Y. Meir, Phys. Rev. B 71 (2005) 035333.
[2] M.A. Reed, C. Zhou, C.J. Muller, T.P. Burgin, J.M. Tour, Science 278 (1997) 252.
[3] S.J. Tans, M.H. Devoret, H. Dai, A. Thess, R.E. Smalley, L.J. Geerligs, C. Dekker, Nature 386 (1997) 474.
[4] D. Goldhaber-Gordon, H. Shtrikman, D. Mahalu, D. Abusch-Magder, U. Meirav, M.A. Kastner, Nature 391 (1998) 56.
[5] D. Goldhaber-Gordon, J. Gores, M.A. Kastner, H. Shtrikman, D. Mahalu, U. Meirav, Phys. Rev. Lett. 81 (1998) 5225.
[6] J. Gores, D. Goldhaber-Gordon, S. Heemeyer, M.A. Kastner, H. Shtrikman, D. Mahalu, U. Meirav, Phys. Rev. B 62 (2000) 2188.
[7] W.J. Liang, M.P. Shores, M. Bockrath, J.R. Long, H. Park, Nature 417 (2002) 725.

[8] J. Park, A.N. Pasupathy, J.I. Goldsmith, C. Chang, Y. Yaish, J.R. Petta, M. Rinkoski, J.P. Sethna, H.D. Abruna, P.L. McEuen, D.C. Ralph, Nature 417 (2002) 722.
[9] T.B. Boykin, R.C. Bowen, G. Klimeck, Appl. Phys. Lett. 75 (1999) 1302.
[10] S. Datta, Superlatt. Microstruct. 28 (2000) 253.
[11] C. Caroli, R. Combescot, P. Nozieres, D. Saint-James, J. Phys. C 4 (1971) 196.
[12] T.B. Boykin, Phys. Rev. B 51 (1995) 4289.
[13] T.B. Boykin, J. Appl. Phys. 78 (1995) 6818.
[14] T.B. Boykin, R.E. Carnahan, R.J. Higgins, Phys. Rev. B 48 (1993) 14232.
[15] R.C. Bowen, G. Klimeck, R.K. Lake, W.R. Frensley, T. Moise, J. Appl. Phys. 81 (1997) 3207.
[16] C. Rivas, R. Lake, G. Klimeck, W.R. Frensley, M.V. Fischetti, P.E. Thompson, S.L. Rommel, P.R. Berger, Appl. Phys. Lett 78 (2001) 814.
[17] H. Li, T. Lu, P. Sun, Phys. Lett. A 343 (2005) 403.
[18] J. Zhu, A.V. Balatsky, Phys. Rev. B 67 (2003) 165326.
[19] Y. Zhang, H. Yu, Y. Gao, J.Q. Liang, Phys. Rev. B 72 (2005) 205310.
[20] Y. Yu, T.C.A. Yeung, W.Z. Shangguan, C.H. Kam, J. Phys.: Condens. Matter 14 (2002) 703.
[21] B. Dong, H.L. Cui, X.L. Lei, Phys. Rev. B 69 (2004) 205315.
[22] D.M.T. Kuo, Physica E 27 (2005) 355.
[23] S. Babiker, IEEE Trans. Electron Devices 52 (2005) 392.
[24] S. Kurth, G. Stefanucci, C.O. Almbladh, A. Rubio, E.K.U. Gross, Phys. Rev. B 72 (2005) 035308.
[25] M. Hornquist, T. Ouchterlony, Physica E 3 (1998) 213.
[26] M. Mardaani, K. Esfarjani, Physica E 27 (2005) 227.
[27] B.K. Nikolic, P.B. Allen, J. Phys.: Condens. Matter 12 (2000) 9629.
[28] W.Z. Shangguan, T.C. Au Yeung, Y.B. Yu, C.H. Kam, Phys. Rev. B 63 (2001) 235323.
[29] R. Lake, G. Klimeck, R.C. Bowen, D. Jovanovic, J. Appl. Phys. 81 (1997) 7845.
[30] Y. Liu, Y. Zheng, W. Gong, W. Gao, T. Lü, Phys. Lett. A 365 (2007) 495.
[31] J.H. Liao, K.J. Chen, L.N. Xu, C.W. Ge, J. Wang, L. Huang, N. Gu, Appl. Phys. A 76 (2003) 541.
[32] J.H. Liao, Y. Zhang, W. Yu, L.N. Xu, C.W. Ge, J.L. Liu, N. Gu, Colloids Surf. A 223 (2003) 177.
[33] D.L. Klein, P.L. Mceuen, J.E.B. Katari, R. Roth, A.P. Alivisatos, Appl. Phys. Lett. 68 (1996) 2574.
[34] F.R. Waugh, M.J. Berry, D.J. Mar, R.M. Westervelt, Phys. Rev. Lett. 75 (1995) 705.